Front. Chem. China 2011, 6(2): 127–141
DOI 10.1007/s11458-011-0236-7

RESEARCH ARTICLE

Vibrational dynamics of Fe-based glassy alloys

Aditya M. VORA

The well recognized model potential is used to investigate the vibrational properties of four Fe-based binary glassy alloys viz. $Fe_{90}Zr_{10}$, $Fe_{80}B_{20}$, $Fe_{83}B_{17}$ and $Fe_{80}P_{20}$. The thermodynamic and elastic properties are also computed from the elastic limits of the phonon dispersion curves (PDC). Three theoretical approaches given by Hubbard-Beeby (HB), Takeno-Goda (TG) and Bhatia-Singh (BS) are used in the present study to compute the PDC. Six local field correction functions proposed by Hartree (H), Taylor (T), Ichimaru-Utsumi (IU), Farid et al. (F) and Sarkar et al. (S) and Sarkar et al.'s local field factor (SLFF) based excgange and correlation function are employed to see the effect of exchange and correlation in the aforesaid properties.

Keywords pseudopotential, pair potential, phonon dispersion curves (PDC), Fe-based binary glassy alloys, static properties, vibrational properties

1 Introduction

The mankind has been manufacturing glassy materials for several thousand years. In conparison, the scientific study of amorphous materials has a much shorter history. And only recently, there has been an explosion of interest to these studies as more promising materials are produced in the amorphous form. The range of applications of metallic glasses is vast and extends from the common window glass e.g. oxide glasses to high capacity storage media for digital devices e.g. chalcogenide glasses involving semiconductor material [1–19].

$Fe_{90}Zr_{10}$ glass is a good example of ferromagnetic glassy material and it is a member of transition metal-transition metal (TM-TM) group. The vibrational dynamics of this glass was studied by Bhandari et al. [11] employing Hubbard-Beeby (HB) [12] and Bhatia-Singh (BS) [13] approaches. They have also calculated the temperature dependence electrical resistivity of $Fe_{90}Zr_{10}$. Also, the structural study of $Fe_{90}Zr_{10}$ glass was made by Hausleitner and Hafner [14] using the MD technique. Recently Wildes et al. [15] have studied the magnetic behavior of $Fe_{90}Zr_{10}$ glass experimentally. The $Fe_{80}B_{20}$, $Fe_{83}B_{17}$ and $Fe_{80}P_{20}$ metallic glasses are the most important candidate of the transition metal-metalloid (TM-M) group. Self-consistent spin-polarized electronic structure of $Fe_{80}B_{20}$ glass has been extensively studied by Hafner et al. [16,17]. The phonon dispersion curves (PDC) of $Fe_{80}B_{20}$ glass has been studied by Gupta et al. [18] employing HB [12] approach. They have compared their findings with available experimental results [18] and found them to be in good agreement with the results. The vibrational dynamics of $Fe_{83}B_{17}$ glass was studied by Saxena [19] using HB [12] approach under model potential formalism. The atomic dynamics of $Fe_{80}P_{20}$ glass has been studied by Hausleitner and Hafner [17]. Recently, we have reported the vibrational properties of some metallic glasses using model potential formalism [1–10].

Looking to the advantages of metallic glasses, the present paper emphasizes the vibrational dynamics of four Fe-based binary glassy alloys, viz. $Fe_{90}Zr_{10}$, $Fe_{80}B_{20}$, $Fe_{83}B_{17}$ and $Fe_{80}P_{20}$ using well known and well recognized model potentials [1–10]. The thermodynamics and elastic properties of longitudinal sound velocity v_L, transverse sound velocity v_T, isothermal bulk modulus B_T, modulus of rigidity G, Poisson's ratio σ, Young's modulus Y and Debye temperature θ_D are computed from the elastic limit of the dispersion relation. Six different types of local field correction functions proposed by Hartree (H) [20], Taylor (T) [21], Ichimaru-Utsumi (IU) [22], Farid et al. (F) [23] and Sarkar et al. (S) [24] are used to study the exchange and correlation effects in the aforesaid studies. The use of appropriate local field factor (LFF) is very important in property calculation of metallic system. Therefore, we have also used most recent Sarkar et al.'s local field factor (SLFF) [25] based exchange and correlation function in the present investigation. Sarkar et al. [25] have recently proposed LFF local field correction function using the quantum Monte Carlo data of Ceperley-Alder for the correlation energy of electron gas in both the "para" and "ferro" states in the given density range. The phenomenological theories of Hubbard-Beeby [12], Takeno-Goda (TG) [26,27] and Bhatia-Singh [13,28] are employed to generate the PDC. The most important ingredient of the PDC is pair potential computed theoretically in Wills-Harrison (WH) [29] form from well recognized model potentials [1–19].

2 Theoretical methodology

The fundamental ingredient, which goes into the calculation of the phonon dynamics of metallic glasses, is the pair potential. In the present study, for TM-TM and TM-M glasses,

Received February 25, 2011; accepted March 11, 2011
Humanities and Social Science Department, STBS College of Diploma Engineering, Surat 395006, India
E-mail: voraam@yahoo.com

the pair potential is computed using [1–19,29],

$$V(r) = V_S(r) + V_b(r) + V_r(r) \quad (1)$$

The s-electron contribution to the pair potential $V_S(r)$ is calculated from

$$V_s(r) = \frac{Z_S^2 e^2}{r} + \frac{\Omega_O}{\pi^2}\int F(q)\frac{\sin(qr)}{qr}q^2 \mathrm{d}q \quad (2)$$

Here Z_s~1.5 is found by integrating the partial s-density of states resulting from self-consistent band structure calculation for the entire 3d and 4d series [29], while Ω_O is the effective atomic volume of the one component fluid.

The energy wave number characteristics appearing in Eq. (2) is written as [1–19,29]

$$F(q) = \frac{-\Omega_O q^2}{16\pi}|W_B(q)|^2 \frac{\varepsilon_H(q)-1}{1+[\varepsilon_H(q)-1][1-f(q)]} \quad (3)$$

Here, $W_B(q)$ is the effective bare ion potential, $\varepsilon_H(q)$ the Hartree dielectric response function and $f(q)$ the local field correction function to introduce the exchange and correlation effects.

The well recognized model potential $W_B(q)$ [1–10] used in the present computation of phonon dynamics of binary metallic glasses is of the form

$$W_B(q) = \frac{-4\pi e^2 Z}{\Omega_O q^2}\left[\begin{array}{l} \left\{\begin{array}{l} -1+\dfrac{12}{U^2}+\dfrac{U^2}{1+U^2}+\dfrac{6U^2}{(1+U^2)^2}+\dfrac{18U^2}{(1+U^2)^3}-\dfrac{6U^4}{(1+U^2)^3} \\ +\dfrac{24U^2}{(1+U^2)^4}-\dfrac{24U^4}{(1+U^2)^4} \end{array}\right\}\cos U \\ +\left\{\begin{array}{l} \dfrac{6}{U}-\dfrac{12}{U^3}+\dfrac{U}{1+U^2}+\dfrac{3U}{(1+U^2)^2}-\dfrac{3U^3}{(1+U^2)^2}+\dfrac{6U}{(1+U^2)^3} \\ -\dfrac{18U^3}{(1+U^2)^3}+\dfrac{6U}{(1+U^2)^4}-\dfrac{36U^3}{(1+U^2)^4}+\dfrac{6U^5}{(1+U^2)^4} \end{array}\right\}\sin U \\ +24U^2\exp(1)\dfrac{U^2-1}{(1+U^2)^4} \end{array}\right] \quad (4)$$

Here $U = qr_C \cdot r_C$ is the model potential parameter. This form has the feature of a Coulombic term outside the core and varying cancellation due to repulsive and attractive contributions to the potential within the core in real space. The detailed information of this potential is given in the literature [1–10]. The model potential parameter r_C is calculated from the well known formula [30] as follows:

$$r_C = \frac{0.51\ r_S}{Z^{1/3}} \quad (5)$$

Here r_S is the Wigner-Seitz radius of the amorphous alloys.

The d-electron contributions to the pair potential are expressed in terms of the number of d-electron Z_d, the d-state radii r_d and the nearest-neighbor coordination number N_C as follows:

$$V_b(r) = -Z_d\left(1-\frac{Z_d}{10}\right)\frac{12}{N_C}\frac{\frac{1}{2}28.06}{\pi}\frac{2r_d^3}{r^5} \quad (6)$$

and

$$V_r(r) = Z_d\left(\frac{450}{\pi^2}\right)\frac{r_d^6}{r^8} \quad (7)$$

The theories of Hubbard-Beeby [12], Takeno-Goda [26,27] and Bhatia-Singh [13,28] have been employed in the present computation. The expressions for longitudinal phonon frequency ω_L and transverse phonon frequency ω_T as per HB, TG and BS approaches are given below [12,13,26–28].

According to the Hubbard-Beeby [12], the expressions for longitudinal phonon frequency ω_L and transverse phonon frequency ω_T are

$$\omega_L^2(q) = \omega_E^2\left[1-\frac{\sin(q\sigma)}{q\sigma}-\frac{6\cos(q\sigma)}{(q\sigma)^2}+\frac{6\sin(q\sigma)}{(q\sigma)^3}\right] \quad (8)$$

and

$$\omega_T^2(q) = \omega_E^2\left[1-\frac{3\cos(q\sigma)}{(q\sigma)^2}+\frac{3\sin(q\sigma)}{(q\sigma)^3}\right] \quad (9)$$

with $\omega_E^2 = \dfrac{4\pi\rho}{3M}\int_0^\infty g(r)V''(r)r^2\mathrm{d}r$ being the maximum frequency.

The theory for computing the phonon dynamics in amorphous solids, an approach proposed by Takeno-Goda [26,27] have been employed in the present computation. The expressions for longitudinal phonon frequency ω_L and transverse phonon frequency ω_T are

$$\omega_L^2(q) = \frac{4\pi\rho}{M}\int_0^\infty \mathrm{d}r g(r)\left\{rV'(r)\left(1-\frac{\sin(qr)}{qr}\right) + \left[r^2V''(r)-rV'(r)\right] \times\left(\frac{1}{3}-\frac{\sin(qr)}{qr}-\frac{2\cos(qr)}{(qr)^2}+\frac{2\sin(qr)}{(qr)^3}\right)\right\} \quad (10)$$

and

$$\omega_T^2(q) = \frac{4\pi\rho}{M}\int_0^\infty \mathrm{d}r g(r)\left\{rV'(r)\left(1-\frac{\sin(qr)}{qr}\right) + \left[r^2V''(r)-rV'(r)\right] \times\left(\frac{1}{3}+\frac{2\cos(qr)}{(qr)^2}+\frac{2\sin(qr)}{(qr)^3}\right)\right\} \quad (11)$$

Here M, ρ are the atomic mass and the number density of the glassy alloy respectively, while $V''(r)$ is the second derivative of the pair potential.

Recently Bhatia-Singh [13] was modified by Shukla and Campnaha [28], and they have introduced screening effects. Then, with the above assumptions and modification, the dispersion equations for an amorphous material can be written as [13,28]

$$\rho\omega_L^2(q) = \frac{2N_C}{q^2}(\beta I_0 + \delta I_2) + \frac{k_e k_{TF}^2 q^2 \varepsilon(q)|G(qr_S)|^2}{q^2 + k_{TF}^2\varepsilon(q)} \quad (12)$$

and

$$\rho\omega_T^2(q) = \frac{2N_C}{q^2}\left(\beta I_0 + \frac{1}{2}\delta(I_0 - I_2)\right) \quad (13)$$

Other used constants in Eqs. (12) and (13) can be found in [13,28]. Here M is the effective atomic mass, ρ is the number density and N_C is the coordination number of the glassy system, respectively.

In the long wavelength limit of the frequency spectrum, both phonon frequencies viz. the longitudinal ω_L and transverse ω_T phonon frequencies are proportional to the wave vectors and obey the relationships [1–13,26–28],

$$\omega_L \propto q \text{ and } \omega_T \propto q$$

$$\therefore \omega_L = v_L q \text{ and } \omega_T = v_T q \quad (14)$$

where, v_L and v_T are the longitudinal and transverse sound velocities of the glassy alloys, respectively. Detailed expressions of the long wavelength limit of the frequency spectrum are narrated in our earlier papers [1–10].

The present study also includes isothermal bulk modulus B_T, modulus of rigidity G, Poisson's ratio σ, Young's modulus Y and Debye temperature θ_D from the elastic limit of the PDC. All the quantities are computed from the longitudinal and transverse sound velocities (v_L and v_T). The bulk modulus B_T, modulus of rigidity G, Poisson's ratio σ, Young's modulus Y and Debye temperature θ_D are obtained using the expressions [1–19]

$$B_T = \rho_M\left(v_L^2 - \frac{4}{3}v_T^2\right) \quad (15)$$

$$G = \rho_M v_T^2 \quad (16)$$

with ρ_M as the isotropic number density of the solid.

$$\sigma = \frac{1-2\left(\frac{v_T^2}{v_L^2}\right)}{2-2\left(\frac{v_T^2}{v_L^2}\right)} \quad (17)$$

$$Y = 2G(\sigma+1) \quad (18)$$

and

$$\theta_D = \frac{\hbar\omega_D}{k_B} = \frac{\hbar}{k_B}2\pi\left(\frac{9\rho}{4\pi}\right)^{1/3}\left(\frac{1}{v_L^3}+\frac{2}{v_T^3}\right)^{-1/3} \quad (19)$$

The low temperature specific heat C_V can be calculated from the following expressions [31],

$$C_V = \frac{\Omega_O\hbar^2}{k_B T^2}\sum_{\lambda=L,T}\int\frac{\mathrm{d}^3q}{(2\pi)^3}\frac{\omega_\lambda^2(q)}{\left[\exp\left(\frac{\hbar\omega_\lambda(q)}{k_BT}\right)-1\right]\left[1-\exp\left(-\frac{\hbar\omega_\lambda(q)}{k_BT}\right)\right]} \quad (20)$$

Here, $\hbar$, k_B, ω_D are the Plank's constant, Boltzmann's constant and Debye frequency, respectively.

3 Results and discussion

The input parameters and other related constants used in the present computations are tabulated in Table 1, which are taken from the literature [29].

The present pair potentials $V(r)$ of $Fe_{90}Zr_{10}$ glass along with those of Bhandari et al. [11] are shown in Fig. 1(a). It is apparent from the figure that the position of the first minimum of the pair potential is greatly affected by the different types of screening functions. The first zero of the pair potential $V(r = r_0)$ due to all screening functions occurs at $r_0 \approx 2.2$ a.u.. The results obtained from S-screening give the maximal well depth. Furthermore, the well depth of presently computed pair

Table 1 Input parameters and other constants.

Glasses	Z	Ω_O/a.u.	r_C/a.u.	Z_d	N_C	r_d/a.u.
Fe_{90} Zr_{10}	3.10	85.39	0.6565	6.10	8.40	1.63
$Fe_{80}B_{20}$	3.00	72.46	0.6363	5.40	8.20	1.41
$Fe_{83}B_{17}$	3.00	73.45	0.6389	5.57	8.17	1.42
$Fe_{80}P_{20}$	3.40	91.88	0.6315	5.40	8.20	1.41

potentials moved toward the left and give a deep potential as compared to Bhandari et al. [11]. The presently computed pair potentials $V(r)$ of $Fe_{80}B_{20}$ glass are shown in Fig. 1(b) with other theoretical data [18,32]. The first zero of the pair potential $V(r = r_0)$ due to H-sceening occurs at $r_0 = 2.09$ a.u., while the exchange and correlation effect suppresses this zero to $r_0 \leqslant 2.3$ a.u.. It is noticed that the position of the well depth of the computed pair potentials $V(r)$ moves toward the left as compared to that of Gupta et al. [18] and Hausleitner-Turek [32] which show higher results than the computed one. The present yielding is not showing any oscillatory behavior. All pair potentials $V(r)$ converge toward the zero at large r-region without any oscillatory behavior. The pair potentials $V(r)$ of binary $Fe_{83}B_{17}$ metallic glass are shown in Fig. 1(c). It is seen that the effect of exchange and correlation functions does not change the nature of the pair potential. The first zero position of pair potential at $r = r_0$ due to all screening functions occurs at $r_0 \approx 2.1$ a.u.. Thus, the effect of inclusion of exchange and correlation on the pair potential $V(r = r_0)$ is not seen substantially. It is observed that the well depth of computed pair potentials moves toward the left and is also higher as compared to that of Saxena [19]. The computed pair potentials $V(r)$ of $Fe_{80}P_{20}$ glass are shown in Fig. 1(d). The first zero for pair potential $V(r = r_0)$ due to all the screening functions occurs at $r_0 \approx 2.09$ a.u.. The maximum depth in the pair potential is obtained for S-function. It is observed that the well depth of presently computed potentials moves toward the left as compared to that of Hausleitner and Hafner [17], whose results are very shallow. The present yielding as well as those of Hausleitner and Hafner [17] do not show any significant oscillations and are almost convergent in the large r-region.

From the Figs. 1(a)–(d), we can observe the shifting of the pair pot pair potentials $V(r)$ with respect to the atomic volume Ω_O of the amorphous alloys. The repulsive coulomb interaction and the attractive interactions represented by oscillatory nature are observed. It is also noticed that when the volume Ω_O of the glassy alloys decreases (Ω_O is less for $Fe_{80}B_{20}$ glass), the potential depth deepens. It means that the pair potentials $V(r)$ for $Fe_{80}B_{20}$ glass show higher depth in comparison with other metallic glasses. All the pair potentials $V(r)$ show the combined effect of the s- and d-electrons. Bretonnet and Derouiche [24] observed that the repulsive part of $V(r)$ is drawn lower and its attractive part is deeper due to the d-electron effect. When we go from $Fe_{83}B_{17} \rightarrow Fe_{90}Zr_{10}$, the net number of d-electron r_d decreases, hence the pair potentials $V(r)$ are shifted toward the lower r -values. Therefore, the present results support the d-electron effect as noted by Bretonnet and Derouiche [33]. Also, from the Figs. 1(a)–(d), it can be noted that the Coulomb repulsive potential part dominates the oscillations due to ion-electron-ion interactions, which shows the oscillatory nature of the potential after $r \approx 10$ a.u.. Hence, the pair potentials converge toward a finite value instead of zero in repulsive region. And, the absence of the oscillatory tail shown in the pair potential is corresponding to only the Friedel's oscillations.

The presently computed pair potentials $V(r)$ using SLFF local field correction function for Fe-based metallic glasses are displayed in Fig. 2. It is clear that the well depth of these glasses is lying between $Fe_{90}Zr_{10}$ and $Fe_{80}P_{20}$ glasses. However, the behavior of $Fe_{80}B_{20}$ and $Fe_{83}B_{17}$ glasses are almost the same and overlapped with each other on the graph. Here also the pair potentials do not show any significant oscillations at larger r -values. It is apparent from the figure that the pair potential for $Fe_{80}P_{20}$ metallic glass shows higher well depth, while that for $Fe_{90}Zr_{10}$ glass presents lower deepness in comparison with the other binary glasses. It is also seen that as Ω_O increases (from $Fe_{90}Zr_{10} \rightarrow Fe_{80}P_{20}$) the depth of the pair potential decreases.

The phonon modes for longitudinal and transverse branches of $Fe_{90}Zr_{10}$, $Fe_{80}B_{20}$, $Fe_{83}B_{17}$ and $Fe_{80}P_{20}$ metallic glasses calculated using HB approach with the five screening functions are shown in Figs. 3–6 The PDC of $Fe_{90}Zr_{10}$ glass obtained using HB approach with all five screening functions is displayed in Fig. 3. The behavior of both the phonon modes has been suppressed after the inclusion of the screening effects. The first minimum in the longitudinal mode for H, T, IU, F and S-local field correction functions is at around $q \approx 3.1$ Å^{-1}, 3.3 Å^{-1}, 3.3 Å^{-1}, 3.3 Å^{-1} and 3.4 Å^{-1}, respectively. The influence of various screening on longitudinal frequency with respect to H-screening is 34.87% for T, 22.17% for IU, 23.02% for F and 27.41% for S-screening. While such influence on ω_T at $q \approx 1.0$ Å^{-1} position is 38.40% for T, 15.94% for IU, 25.82% for F and 32.74% for S-screening function. In the present study the phonon eigen frequencies for longitudinal and transverse phonon modes of $Fe_{80}B_{20}$ glass calculated using HB approach with all five screening

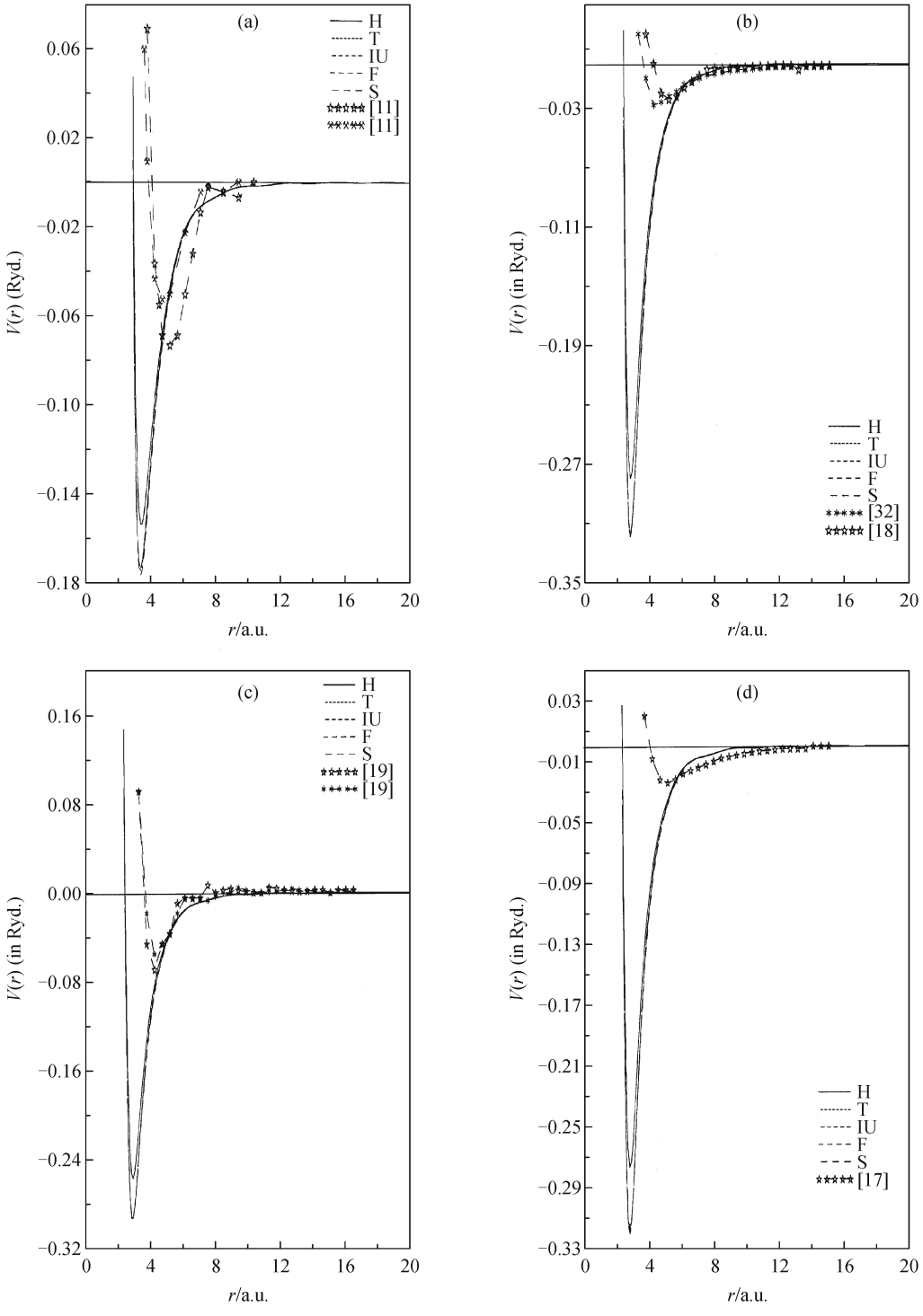

Figure 1 Pair potentials for (a) $Fe_{90}Zr_{10}$, (b) $Fe_{80}B_{20}$, (c) $Fe_{83}B_{17}$ and (d) $Fe_{80}P_{20}$ metallic glasses

functions are shown in Fig. 4. It is evident that the influence of exchange and correlation effects suppresses both phonon frequencies for low wave vector region. The first minimum occurs in the longitudinal branch at $q \approx 3.5$ Å^{-1}, 3.8 Å^{-1}, 3.8 Å^{-1}, 3.8 Å^{-1} and 3.9 Å^{-1} for H, T, IU, F and S-local field correction functions, respectively. The influence of various screening functions at the first maximum of ω_L with respect to H-screening is 4.94% for T, 3.00% for IU, 2.76% for F and 53.55% for S-screening. Such screening influence observed at $q \approx 1.0$ Å^{-1} in transverse branch for T, IU, F and S-function is

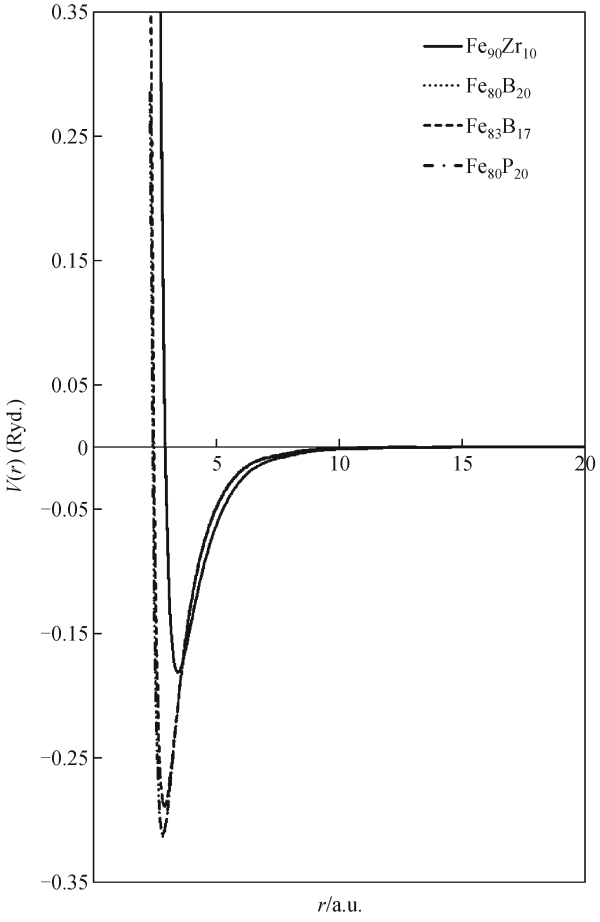

Figure 2 Pair potentials for Fe-based metallic glasses using SLFF-local field correction function

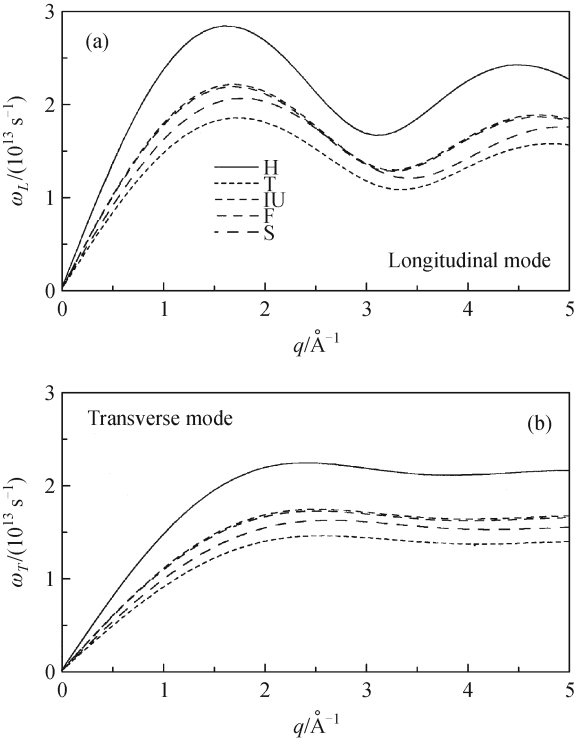

Figure 3 Screening dependence of the phonon dispersion curves for $Fe_{90}Zr_{10}$ metallic glasses using HB approach

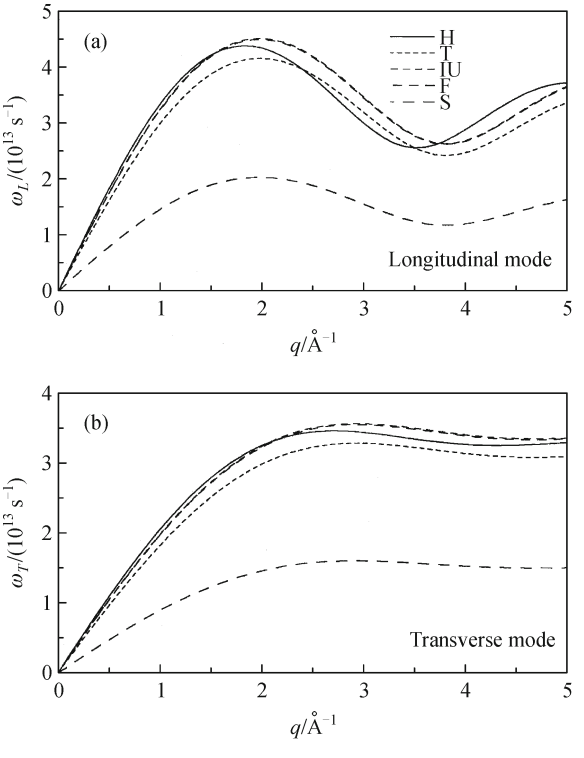

Figure 4 Screening dependence of the phonon dispersion curves for $Fe_{80}B_{20}$ metallic glasses using HB approach

11.20%, 3.63%, 4.00% and 56.41% in comparison to the static H-dielectric function, respectively. The phonon eigen frequencies of $Fe_{83}B_{17}$ glass calculated using HB approach with the five screening functions are displayed in Fig. 5 which help us to study screening influence on the aforesaid properties. The first depth in the longitudinal branch is at around 1.7 Å^{-1} for H, 2.6 Å^{-1} for T as well as IU, 2.5 Å^{-1} for F and 1.7 Å^{-1} for S-local field correction function. The screening influence at the first maximum of ω_L is 9.07% for T, 0.00% for IU, 0.44% for F and 55.43% for S-screening with respect to H-screening, which does not include any exchange and correlation effects. Such influence on ω_T at $q \approx 1.0$ Å^{-1} position is 16.27% for T, 7.92% for IU, 8.32% for F and 59.53% for S-screening, respectively. The PDC of $Fe_{80}P_{20}$ glass is not reported by others until our literature survey. To show the screening influence on the eigen frequencies Fig. 6 is drown where the results of HB approach are used. It is apparent from the figure that the influence of exchange and correlation effects suppresses the phonon frequencies in both longitudinal and transverse branches. The first minimum in

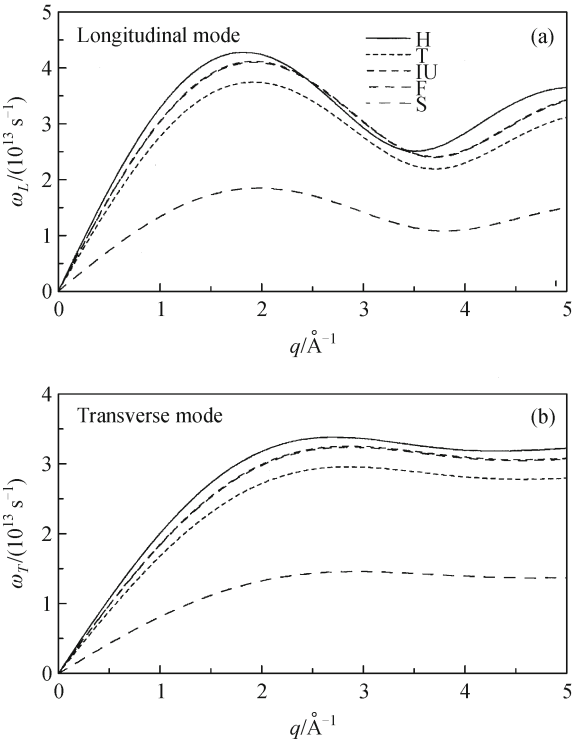

Figure 5 Screening dependence of the phonon dispersion curves for $Fe_{83}B_{17}$ metallic glasses using HB approach

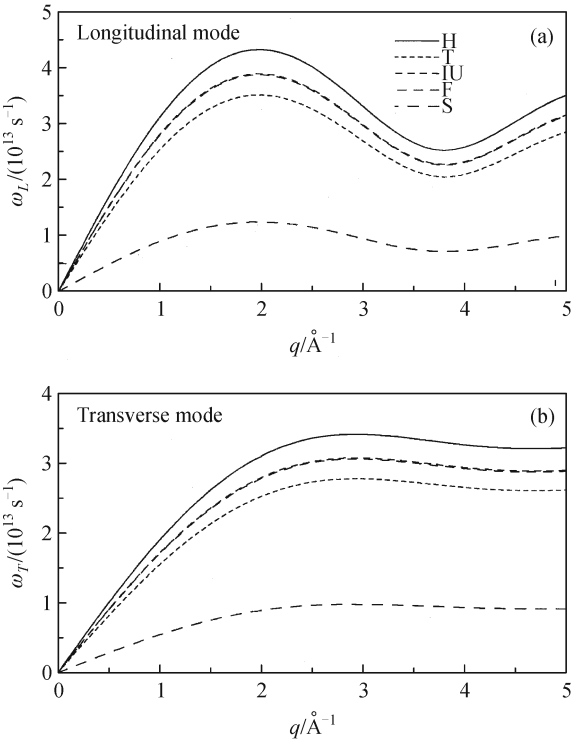

Figure 6 Screening dependence of the phonon dispersion curves for $Fe_{80}P_{20}$ metallic glasses using HB approach

the longitudinal branch for H, T, IU, F and S-local field correction functions is at around $q \approx 3.8$ Å^{-1}, 3.8 Å^{-1}, 3.8 Å^{-1}, 3.8 Å^{-1} and 3.8 Å^{-1}, respectively. As compared to previously reported metallic glasses, the influence of T, IU and F on ω_L is small. Such influence ranges from 9.94% to 18.05%. The S-function enhances the ω_L of $Fe_{80}P_{20}$ glass by about 71.74% in comparison with H-dielectric function. While the influence of screening at $q \approx 1.0$ Å^{-1} point on transverse mode is 18.65% for T, 9.94% for IU, 10.37% for F and 71.14% for S-screening with respect to H-screening.

The PDC obtained from three approaches viz. HB, TG and BS with S-function of $Fe_{90}Zr_{10}$ glass are plotted in Fig. 7(a) and show the characteristic behavior of dispersion relation in a disordered system. The present outcome due to HB and TG approaches is low in comparison with the reported data [11]. The first deepness in the longitudinal branch is observed at $q \approx 3.4$ Å^{-1} for HB, $q \approx 1.9$ Å^{-1} for TG and $q \approx 1.5$ Å^{-1} for BS approach. The first crossing position of ω_L and ω_T in the HB, TG and BS approaches is found, respectively at 2.8 Å^{-1}, 1.3 Å^{-1} and 1.4 Å^{-1}. The PDC obtained due to three approaches of $Fe_{80}B_{20}$ glass is shown in Fig. 7(b). The first depth in the longitudinal branch falls at $q \approx 3.9$ Å^{-1} for HB, $q \approx 2.3$ Å^{-1} for TG and $q \approx 1.5$ Å^{-1} for BS approach. The first crossing position of ω_L and ω_T in the HB, TG and BS approaches is observed, respectively, at 2.9 Å^{-1}, 1.7 Å^{-1} and 1.4 Å^{-1}. The results from BS approach are very high in contrast to TG and HB approaches. The present yielding is found in line with other theoretical and experimental data [18]. The PDC obtained from three approaches viz. HB, TG and BS with S-function of $Fe_{83}B_{17}$ glass is apparent in Fig. 7 (c) and show the characteristic behavior of dispersion relation in a disordered system. The present outcome from HB and TG approaches is very low in comparison with the reported theoretical and experimental data [19]. The first minimum in the longitudinal branch lies at $q \approx 3.8$ Å^{-1} for HB, $q \approx 2.3$ Å^{-1} for TG and $q \approx 1.5$ Å^{-1} for BS approach. The first intersect point of both the phonon frequencies in HB, TG and BS approaches is seen at 2.9 Å^{-1}, 1.8 Å^{-1} and 1.4 Å^{-1}, respectively. The PDC from the three approaches (HB, TG, BS) of $Fe_{80}P_{20}$ glass with S-local field correction function are shown in Fig. 7(d). It is seen that the oscillations is prominent in the longitudinal phonon modes as compared to the transverse modes. The present outcome of PDC from BS approach is higher than those from HB and TG approaches. The first minimum in the longitudinal branch occurs at $q \approx 3.8$ Å^{-1}, $q \approx 2.2$ Å^{-1} and $q \approx 1.5$ Å^{-1}, for HB, TG and BS approaches, respectively. The first crossover location of both the phonon branches is seen at 2.9 Å^{-1}, 1.7 Å^{-1} and 1.4 Å^{-1}, respectively, in HB, TG and BS approaches.

The phonon modes for longitudinal and transverse branches of $Fe_{90}Zr_{10}$, $Fe_{80}B_{20}$, $Fe_{83}B_{17}$ and $Fe_{80}P_{20}$ metallic

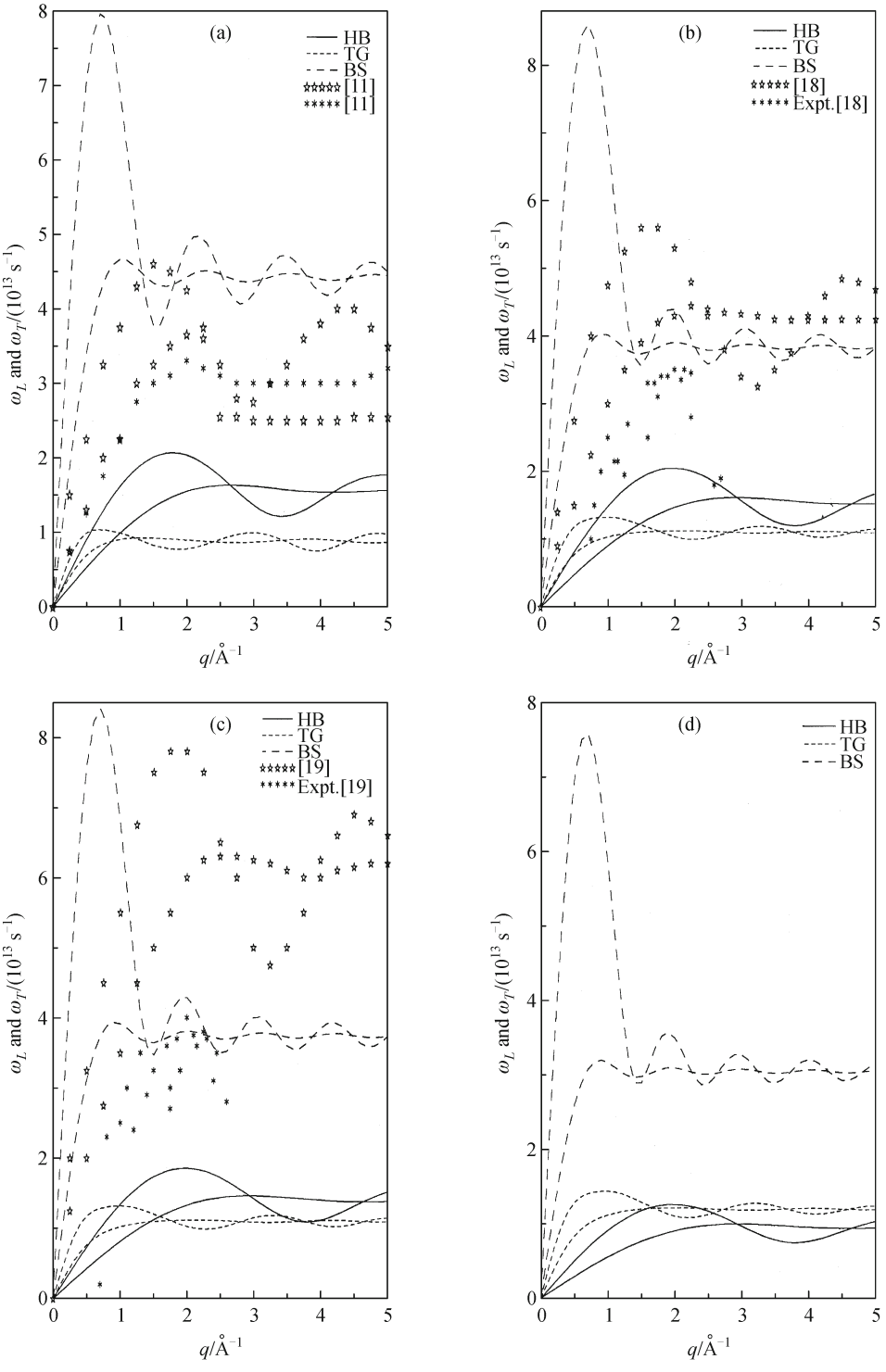

Figure 7 Phonon dispersion curves for (a) $Fe_{90}Zr_{10}$, (b) $Fe_{80}B_{20}$, (c) $Fe_{83}B_{17}$ and (d) $Fe_{80}P_{20}$ metallic glasses using HB, TG and BS approaches with S-local field correction function

glasses calculated using three approaches with SLFF [25] based exchange and correlation function are shown in Figs. 8(a)–(d). The PDC obtained from three approaches viz. $Fe_{90}Zr_{10}$ glass is plotted in Fig. 8(a) and show the characteristic behavior of dispersion relation in a disordered system. The present outcome from HB and TG approaches are low in comparison with the reported data [11]. The first deepness in the longitudinal branch is observed at $q \approx 3.9$ Å^{-1} for HB, $q \approx 2.2$ Å^{-1} for TG and $q \approx 1.5$ Å^{-1} for BS approach. The first crossing position of ω_L and ω_T in HB, TG and BS

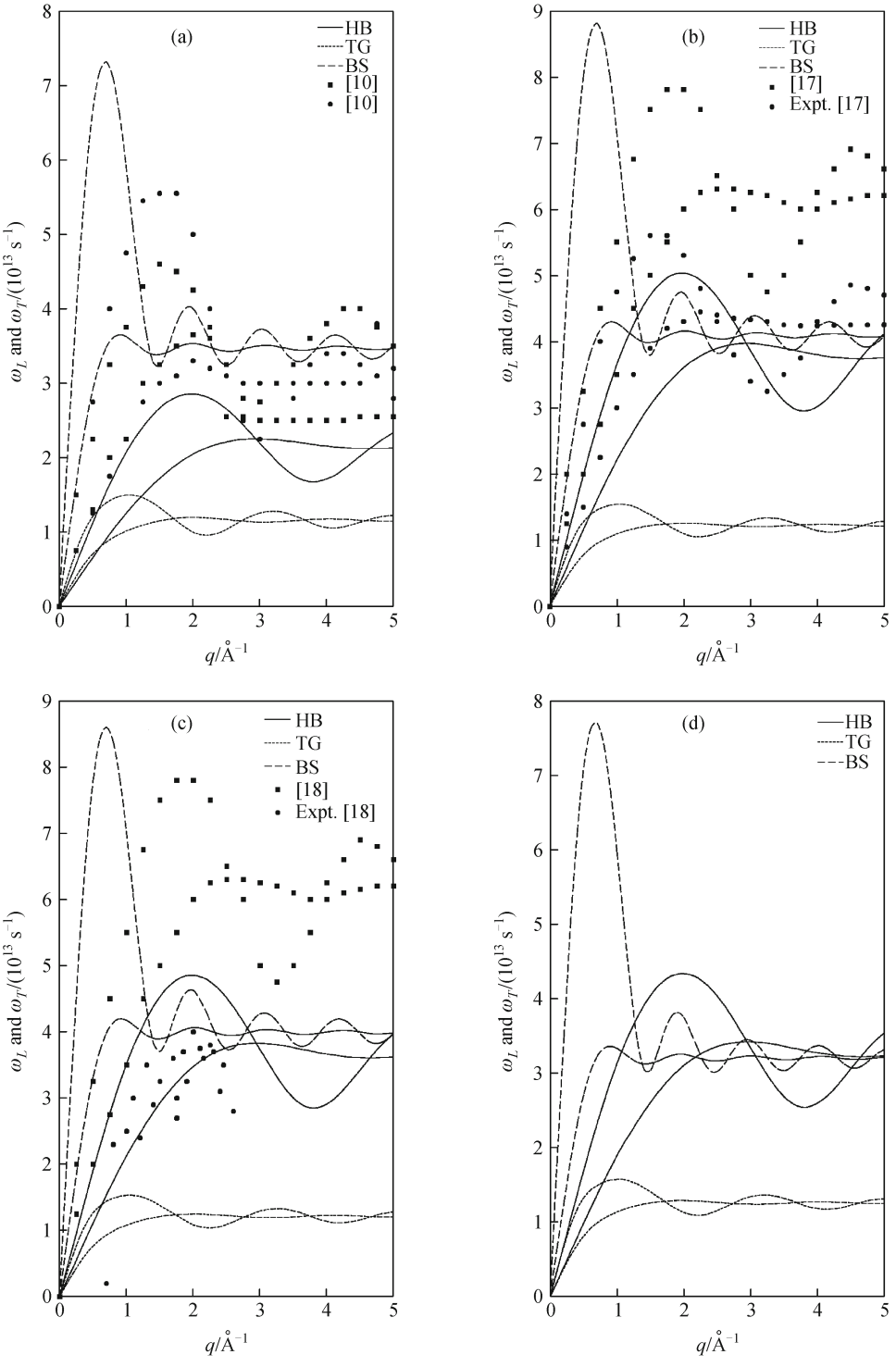

Figure 8 Phonon dispersion curves for (a) $Fe_{90}Zr_{10}$, (b) $Fe_{80}B_{20}$, (c) $Fe_{83}B_{17}$ and (d) $Fe_{80}P_{20}$ metallic glasses using HB, TG and BS approaches with SLFF-local field correction function

approaches is found, respectively, at 2.9 $Å^{-1}$, 1.7 $Å^{-1}$ and 1.4 $Å^{-1}$. The PDC obtained from the three approaches of $Fe_{80}B_{20}$ glass is shown in Fig. 8(b). The first depth in the longitudinal branch falls at $q \approx 3.8$ $Å^{-1}$ for HB, $q \approx 2.2$ $Å^{-1}$ for TG and $q \approx 1.5$ $Å^{-1}$ for BS approach. The first crossing position of ω_L and ω_T in HB, TG and BS approaches is observed, respectively, at 2.9 $Å^{-1}$, 1.7 $Å^{-1}$ and 1.4 $Å^{-1}$. The results from BS approach are very high in contrast to TG and HB approaches. The present yielding is found in line with other theoretical and experimental data [18]. The PDC

obtained from three approaches viz. HB, TG and BS with S-function of $Fe_{83}B_{17}$ glass is apparent in Fig. 8(c) and show the characteristic behavior of dispersion relation in a disordered system. The present outcome from HB and TG approaches are very low in comparison with the reported theoretical and experimental data [19]. The first minimum in the longitudinal branch lies at $q \approx 3.8$ Å^{-1} for HB, $q \approx 2.3$ Å^{-1} for TG and $q \approx 1.5$ Å^{-1} for BS approach. The first intersect point of both phonon frequencies in HB, TG and BS approaches is seen at 3.0 Å^{-1}, 1.7 Å^{-1} and 1.4 Å^{-1}, respectively. The PDC from the three approaches (HB, TG, BS) of $Fe_{80}P_{20}$ glass with S-local field correction function is shown in Fig. 8(d). It is seen that the oscillations are prominent in the longitudinal phonon modes as compared to the transverse modes. The present outcomes of PDC from BS approach are higher than those from HB and TG approaches. The first minimum in the longitudinal branch occurs at $q \approx 3.8$ Å^{-1}, $q \approx 2.2$ Å^{-1} and $q \approx 1.4$ Å^{-1}, for HB, TG and BS approaches, respectively. The first crossover location of both phonon branches is seen at 2.9 Å^{-1}, 1.7 Å^{-1} and 1.4 Å^{-1}, respectively, in HB, TG and BS approaches.

It is observed from Figs. 7(a)–(d) and Figs. 8(a)–(d) that, the first peak position of longitudinal branch of $Fe_{80}B_{20}$ glass is higher while that of $Fe_{80}P_{20}$ glass is lower in comparison with other metallic glasses. The lower dip in the longitudinal branch justifies the correctness and stability of the pair potential. The same results are observed in transverse branch as well. Moreover, it is observed from Figs. 7(a)–(d) and Figs. 8(a)–(d) that, the oscillations are more prominent in the longitudinal phonon modes as compared to the transverse modes. This shows the existence of collective excitations at larger momentum transfer due to longitudinal phonons only and the instability of the transverse phonons due to the anharmonicity of the atomic vibrations in the metallic systems. Also in the high wave vector region, damping of phonons dominates the transverse mode, indicating the fluid characteristic of the glass, i.e., the transverse phonon behavior is monotonic. Here in transverse branch, the frequencies increase with the wave vector q and then saturates at $\approx q$ = 2.0 Å^{-1}. It supports the well known Thorpe model [34] which describes a glass as a solid containing finite liquid cluster. The transverse phonons are absorbed for frequencies larger than the smallest eigen frequencies of the largest cluster. We have observed some common features and small difference between the results obtained from standard S and SLFF local field correction functions. Therefore, we cannot deduce general remarks from the present study.

Generally, collective density waves have been measured at larger momenta, and for some metallic glasses it has been possible to follow the dynamical structure factor out to very large wave vectors. Characteristically, the dispersion relations derived from these dynamical structure factors show a minimum near q_P, the wave vector where the static structure factor $S(q)$ of the glass has its first maximum. But, in the present case, we have not found any type of structural data related to the metallic glasses. Therefore, we have not included structural data in the graph of the PDC.

As shown in Figs. 9–12 for $Fe_{90}Zr_{10}$, $Fe_{80}B_{20}$, $Fe_{83}B_{17}$ and $Fe_{80}P_{20}$ metallic glasses, the exchange and correlation functions also affected the anomalous behavior, (i.e., deviation from the T^3 law), which is observed in the vibrational part of the low temperature specific heat C_V. The reason behind the anomalous behavior may be that the low frequency modes modify the generalized vibrational density of the states of the glass with that of the polycrystal. These modes are mainly responsible for the difference in the temperature dependence of the vibrational part of the specific heat which departs from the normal behavior. The existence of a portion of the spectrum with "softer phonons" (resembling rotons in liquid helium) may account for the anomalous behavior of low temperature specific heat C_V. In the low temperature region, a contribution to the low temperature specific heat C_V is made by phonons of the initial part of the frequency spectrum. When the temperature reaches a value at which the energy of the thermal motions becomes comparable to the energy of "softer phonons" minimum, an additional contribution is made to the heat capacity from the roton portion of the phonon frequency $\omega(q)$. Here also, C_V/T rises initially within low temperature range in HB and TG approaches and then falls sharply with further increase in temperature. Such a high fluctuation in $C_V/T \rightarrow T^2$ curve at low temperature is absent in BS approach.

Furthermore, the thermodynamic and elastic properties of Fe-based glassy alloys estimated from the elastic limit of the PDC are tabulated in Tables 2–5. From Table 2, it is noted that the present outcomes of these properties of $Fe_{90}Zr_{10}$ glass are found in line with other such reported data [11]. It is seen from Table 3 that the screening theory plays an important role in the prediction of the thermodynamic and elastic properties of $Fe_{80}B_{20}$ glass. As phonon modes obtained for BS approach is very high compared to HB and TG approaches, the thermodynamic and elastic properties obtained for BS approach is also higher in magnitude compared to HB and TG approaches. The present results are found in qualitative agreement with the available experimental [18] or theoretical [18] data. The thermodynamic and elastic properties are calculated from the elastic part of the PDC and narrated in Table 4 for $Fe_{83}B_{17}$ glass. It is noticed that the properties are very sensitive to screening functions used. The v_L and v_T from S-screening show low values in HB and TG approaches while

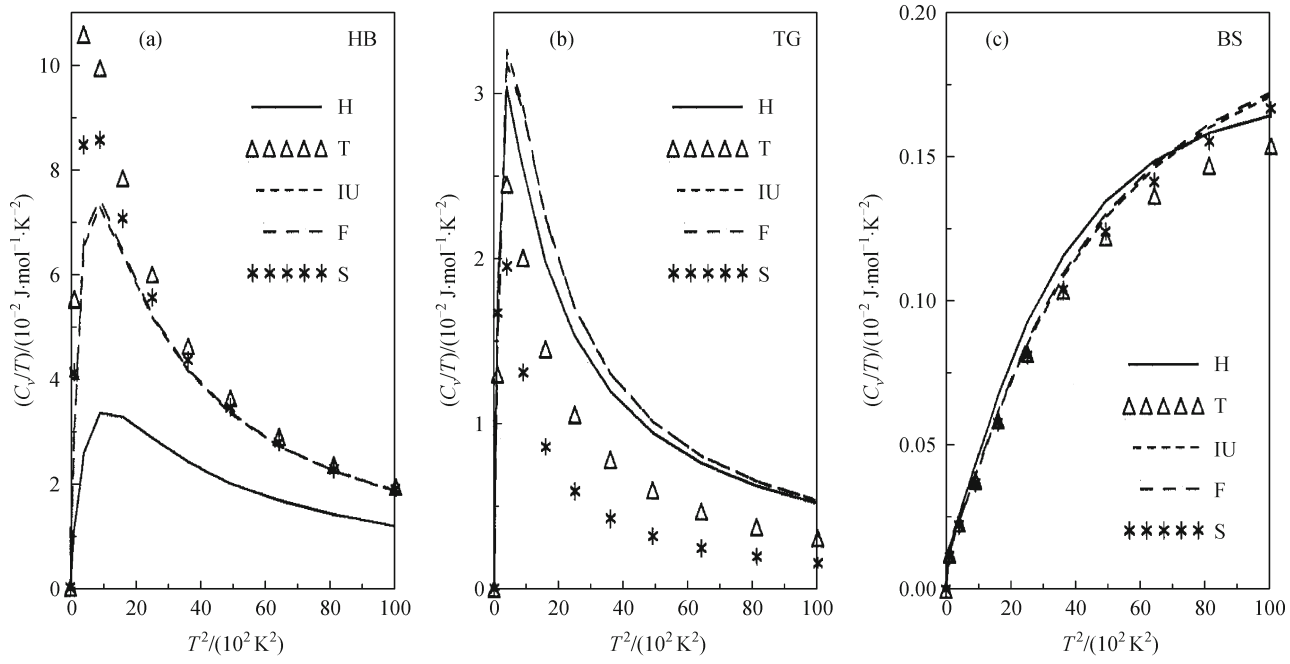

Figure 9 Screening dependence of the low temperature specific heat for $Fe_{90}Zr_{10}$ metallic glasses computed from HB, TG and BS approaches

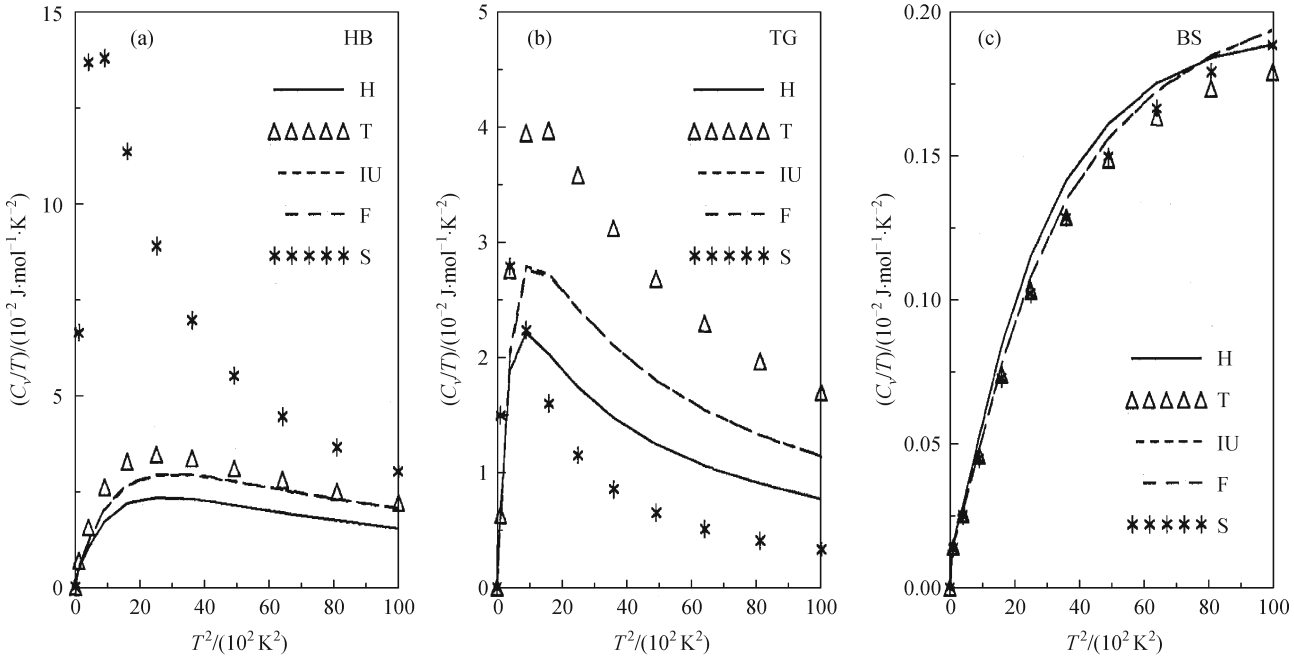

Figure 10 Screening dependence of the low temperature specific heat for $Fe_{80}B_{20}$ metallic glasses computed from HB, TG and BS approaches

high values in BS approach as compared to other screening. Moreover, both the velocities give the fair results from BS approach compare to others [19] while B_T gives good agreement in TG approach compare to experimental and other results [19]. Also, BS approach provides good results for Y as compared to experimental and other data [19]. The thermodynamic and elastic properties of $Fe_{80}P_{20}$ glass are also computed and reported in Table 5. Here for BS approach, the

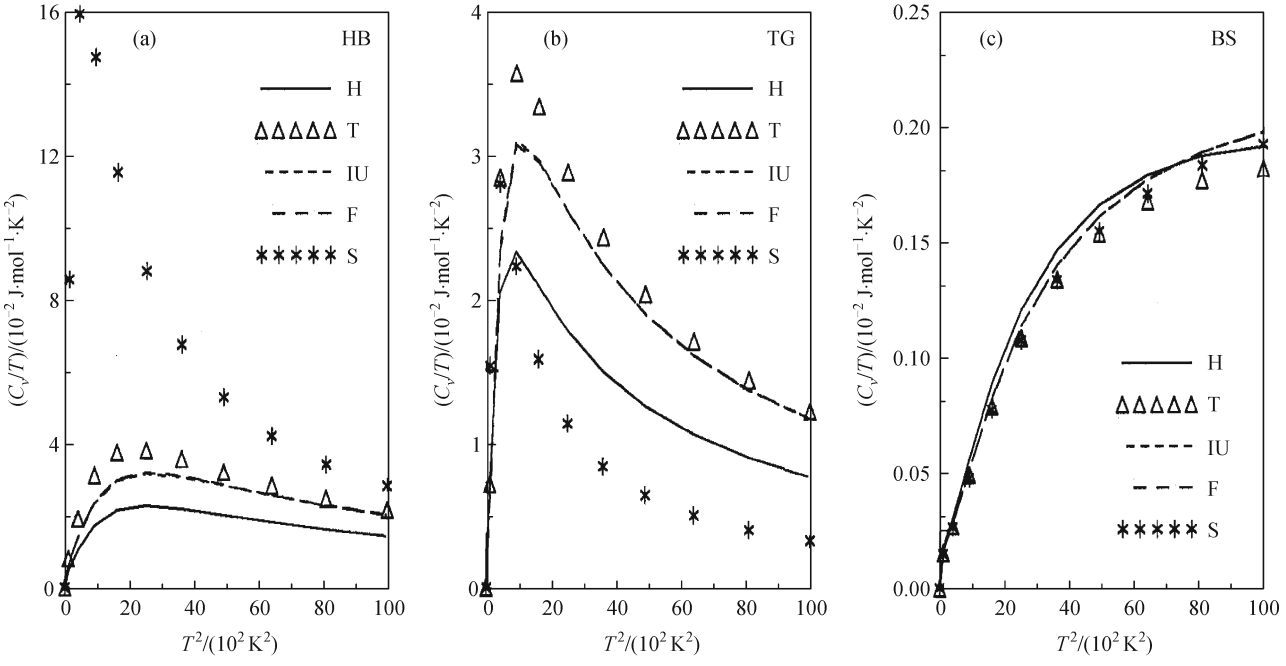

Figure 11 Screening dependence of the low temperature specific heat for $Fe_{83}B_{17}$ metallic glasses computed from HB, TG and BS approaches

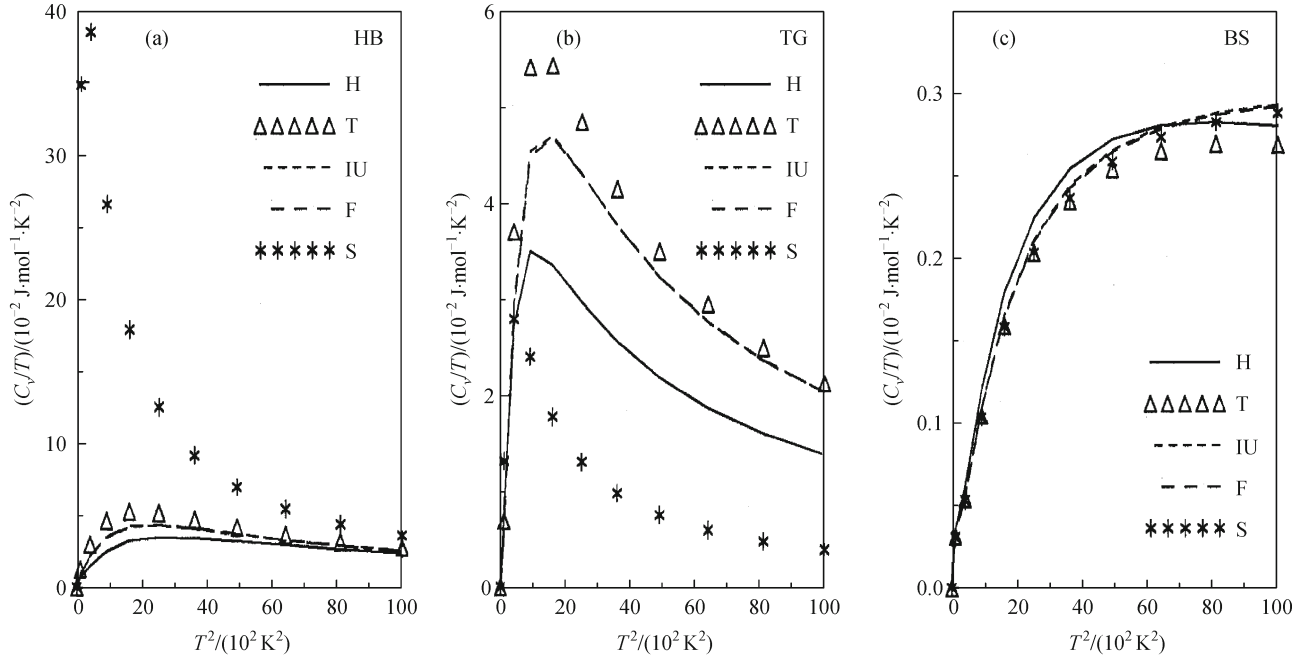

Figure 12 Screening dependence of the low temperature specific heat for $Fe_{80}P_{20}$ metallic glasses computed from HB, TG and BS approaches

results obtained for υ_L, υ_T, B_T, G, σ, Y and θ_D are very high compared to TG and HB approaches. The screening influence on the PDC is reflected on these properties as well.

The dielectric function plays an important role in the evaluation of potential due to the screening of the electron gas. For this purpose, in the present investigation, the local field

Table 2 Thermodynamic and elastic properties of $Fe_{90}Zr_{10}$ glass

App.	SCR	v_L /(10^5 cm·s^{-1})	v_T /(10^5 cm·s^{-1})	B_T /(10^{11} dyne·cm^{-2})	G /(10^{11} dyne·cm^{-2})	σ	Y /(10^{11} dyne·cm^{-2})	θ_D/K
	H	2.8073	1.6208	3.4113	2.0468	0.2499	5.1170	230.01
	T	1.7072	0.9856	1.2616	0.7569	0.2500	1.8924	139.87
HB	IU	2.0871	1.2050	1.8857	1.1314	0.2499	2.8285	171.00
	F	2.0645	1.1920	1.8450	1.1070	0.2499	2.7675	169.15
	S	1.8562	1.0717	1.4915	0.8949	0.2499	2.2373	152.09
	H	3.7509	1.6695	8.0669	2.1717	0.3765	5.9785	240.80
	T	3.3855	1.9186	5.1063	2.8682	0.2634	7.2476	272.71
TG	IU	3.5793	1.8849	6.2908	2.7684	0.3081	7.2428	269.41
	F	3.6178	1.9227	6.3573	2.8805	0.3032	7.5076	274.63
	S	2.8751	1.6987	3.4428	2.2484	0.2318	5.5394	240.56
	H	8.7030	3.7767	44.1979	11.1135	0.3840	30.7620	545.29
	T	8.8698	3.9556	45.0447	12.1914	0.3759	33.5475	570.48
BS	IU	8.8507	3.9295	44.9946	12.0312	0.3772	33.1399	566.83
	F	8.8301	3.9118	44.8551	11.9231	0.3779	32.8580	564.33
	S	8.9135	4.0007	45.2779	12.4709	0.3739	34.2667	576.83
Expt [11].		–	–	–	–	–	–	16.66
Others [11]			4.8 6.2	2.81 2.35	9.60 23.8	6.05 4.23	0.23 0.41	15.01 12.00

Table 3 Thermodynamic and elastic properties of $Fe_{80}B_{20}$ glass

App.	SCR	v_L /(10^5 cm·s^{-1})	v_T /(10^5 cm·s^{-1})	B_T /(10^{11} dyne·cm^{-2})	G /(10^{11} dyne·cm^{-2})	σ	Y /(10^{11} dyne·cm^{-2})	θ_D/K
	H	3.8570	2.2268	5.9849	3.5909	0.2500	8.9773	333.79
	T	3.3861	1.9550	4.6128	2.7677	0.2499	6.9192	293.04
HB	IU	3.6747	2.1216	5.4324	3.2594	0.2499	8.1486	318.01
	F	3.6605	2.1134	5.3905	3.2343	0.2499	8.0857	316.78
	S	1.6619	0.9595	1.1111	0.6666	0.2499	1.6666	143.82
	H	4.8530	2.0830	12.8652	3.1420	0.3871	8.7164	317.80
	T	4.6937	2.2569	11.0351	3.6885	0.3496	9.9563	342.58
TG	IU	4.9114	2.2747	12.4718	3.7470	0.3635	10.2178	345.93
	F	4.9432	2.3088	12.5474	3.8602	0.3605	10.5035	350.98
	S	3.2967	1.8910	4.4175	2.5895	0.2548	6.4987	283.61
	H	9.4947	3.5570	53.0644	9.1621	0.4184	25.9906	545.01
	T	9.6119	3.7067	53.6360	9.9496	0.4127	28.1106	567.51
BS	IU	9.5753	3.6666	53.4138	9.7351	0.4141	27.5327	561.47
	F	9.5725	3.6662	53.3784	9.7331	0.4141	27.5263	561.41
	S	9.6453	3.7405	53.8594	10.1317	0.4115	28.6016	572.59
Expt [18].			4.773	–	1.41	0.65	0.3	1.69
Others [18]			5.15	3.05	1.04 1.38	0.688 0.50	0.229	1.693

correction functions due to H, T, IU, F, S and SLFF are used. The reason for selecting these functions is that H-function does not include exchange and correlation effect and represents only static dielectric function, while T-function covers the overall features of the various local field correction functions proposed before 1972. IU, F and S-functions are recent ones among the existing functions and not exploited rigorously in such studies. This helps us to study the relative effects of exchange and correlation in the aforesaid properties. Hence, the five different local field correction functions show variations up to an order of magnitude in all the properties. Also, the use of appropriate local field factor is very important in property calculation of ferroalloy and their magnetic properties. Therefore, in the present work we have also used most recent Sarkar et al.'s local field factor [25] based exchange and correlation function. Basically, it is proposed by

Table 4 Thermodynamic and elastic properties of $Fe_{83}B_{17}$ glass

App.	SCR	v_L /(10^5 cm·s^{-1})	v_T /(10^5 cm·s^{-1})	B_T /(10^{11} dyne·cm^{-2})	G /(10^{11} dyne·cm^{-2})	σ	Y /(10^{11} dyne·cm^{-2})	θ_D/K
	H	3.7563	2.1687	5.7613	3.4568	0.2500	8.6419	323.60
	T	3.1207	1.8018	3.9765	2.3859	0.2499	5.9648	268.85
HB	IU	3.4322	1.9816	4.8099	2.8860	0.2499	7.2149	295.68
	F	3.4170	1.9728	4.7674	2.8604	0.2500	7.1511	294.37
	S	1.5026	0.8675	0.9219	0.5532	0.2500	1.3829	129.45
	H	4.7506	2.0302	12.5478	3.0293	0.3883	8.4110	308.39
	T	4.4761	2.2065	9.9540	3.5783	0.3395	9.5861	332.96
TG	IU	4.6931	2.2194	11.3607	3.6201	0.3560	9.8176	335.65
	F	4.7259	2.2538	11.4368	3.7332	0.3528	10.1006	340.70
	S	3.2662	1.8710	4.4105	2.5727	0.2558	6.4617	279.37
	H	9.3156	3.4901	51.8441	8.9522	0.4184	25.3949	532.34
	T	9.4301	3.6364	52.3994	9.7186	0.4127	27.4582	554.23
BS	IU	9.3938	3.5965	52.1792	9.5065	0.4141	26.8867	548.26
	F	9.3911	3.5962	52.1445	9.5048	0.4141	26.8811	548.20
	S	9.4631	3.6696	52.6193	9.8971	0.4115	27.9395	559.21
Expt [19].		–	–	17.0	–	–	20.6	555±90
Others [19]		6.0	4.0	10.2	–	–	24.447	599

Table 5 Thermodynamic and elastic properties of $Fe_{80}P_{20}$ glass

App.	SCR	v_L /(10^5 cm·s^{-1})	v_T /(10^5 cm·s^{-1})	B_T /(10^{11} dyne·cm^{-2})	G /(10^{11} dyne·cm^{-2})	σ	Y /(10^{11} dyne·cm^{-2})	θ_D/K
	H	3.5222	2.0335	4.2746	2.5648	0.2500	6.4119	281.62
	T	2.8654	1.6543	2.8290	1.6974	0.2500	4.2434	229.10
HB	IU	3.1721	1.8314	3.4670	2.0802	0.2500	5.2005	253.62
	F	3.1569	1.8227	3.4340	2.0604	0.2499	5.1510	252.41
	S	1.0164	0.5868	0.3560	0.2136	0.2500	0.5340	81.27
	H	4.7945	2.1277	10.5135	2.8078	0.3774	7.7348	299.52
	T	4.5387	2.3845	8.0744	3.5265	0.3094	9.2351	332.64
TG	IU	4.7384	2.3882	9.2092	3.5372	0.3297	9.4073	334.03
	F	4.7800	2.4282	9.2950	3.6568	0.3261	9.6986	339.46
	S	3.5755	2.0416	4.4819	2.5852	0.2581	6.5048	283.00
	H	9.0302	3.0378	42.9431	5.7234	0.4362	16.4399	431.05
	T	9.1310	3.1774	43.3614	6.2616	0.4311	17.9222	450.57
BS	IU	9.0970	3.1397	43.1741	6.1138	0.4324	17.5148	445.29
	F	9.1036	3.1492	43.1989	6.1509	0.4320	17.6165	446.62
	S	9.1448	3.1909	43.4469	6.3148	0.4307	18.0690	452.45

using the quantum Monte Carlo data of Ceperley-Alder for the correlation energy of electron gas in both the "para" and "ferro" states, in the given density range.

HB approach is the simplest and older theory, which has generated consistent results of the phonon data of the glassy systems because this approach needs a minimum number of input parameters. While TG approach leads us to a self-consistent treatment for phonon eigen values because the phonon eigen frequencies are determined by effective force constant, which depends upon the correlation function for the displacement of atoms in solids, whereas the correlation function of displacement itself depends on the phonon frequencies. BS approach has retained the interatomic interactions of the atoms, effective only between the first nearest neighbors. Hence, there is a severer disorder of the atoms in the formation of metallic glasses, which shows deviation in magnitude of the PDC and their related vibrational properties. From the present study we have concluded that all three approaches are suitable for the study of the vibrational dynamics of the amorphous materials. Hence, successful application of the model potential with three approaches is observed from the present study. The

collective excitations in alloys strongly depend on the repulsive part of the pair potentials. The collective excitations are persistent if the repulsion is soft, whereas these excitations are not supported by hard repulsive potentials. The results of the pair potentials and the PDCs seem contradictory to this because of the effect of model potential and local field correction functions. Therefore, the pair potentials used show the hard repulsive part. Still, the longitudinal PDCs phonons are persistent for quite a long q range.

4 Conclusions

Finally, it is concluded that in the study of phonon dynamics of metallic glasses, the pair potentials and its derivatives as well as pair correlation function plays an important role. In the present computation, the WH form is adopted to generate the pair potentials, which ignores the angular interaction due to partially filled d-bands in transition metals. Most recent model potential with WH model and HB approach produces consistent results of phonon dynamics for all metallic glasses. Hence, the present model potential is suitable for studying the phonon dynamics of four Fe-based metallic glasses, which confirms the applicability of the model potential in the aforementioned study. Such study on phonon dynamics of other binary as well as ternary liquid alloys and metallic glasses is in progress, which will be communicated in the near future.

References

1. Vora, A. M.; Patel, M. H.; Gajjar, P. N.; Jani, A. R., *Solid State Phys*. **2003**, *46*, 315
2. Gajjar, P. N.; Vora, A. M.; Jani, A. R., In: Proceedings of the 9th Asian Pacific Physics Conference Hanoi, The Gioi Publication, Vietnam 2006, 429
3. Vora, A. M., *Chin. Phys. Lett*. **2006**, *23*, 1872–1875
4. Vora, A. M., *J. Mater. Sci*. **2007**, *43*, 935–940
5. Vora, A. M., *Acta Physiol. Pol*. **2007**, *A111*, 859
6. Aditya, M. Vora, J. Non-Cryst., *Sol*. **2006**, *352*, 3217
7. Vora, A. M., *Front. Mater. Sci. China* **2007**, *1*, 366–378
8. Vora, A. M., *FIZIKA* **2007**, *A16*, 187
9. Vora, A. M., *Rom. J. Physiol*. **2008**, *53*, 517
10. Vora, A. M., *Front. Mater. Sci. China* **2009**, *3*, 285–300
11. Bhandari, D.; Prasad, A.; Gupta, A.; Saxena, N. S., in *The Physics of Disordered Materials*, Saksena, M. P., Saxena, N. S., Bhandari, D. (Eds.), NISCOM, New Delhi, 1997, pp. 86–90.
12. Hubbard, J.; Beeby, J. L.; *J. Phys. C: Solid State Phys*. **1969**, *2*, 556–571
13. Bhatia, A. B.; Singh, R. N., *Phys. Rev. B* **1985**, *31*, 4751–4758
14. Hausleitner, Ch.; Hafner, J.; Non-Cryst, J., *Sol*. **1992**, *144*, 175
15. Wildes, A. R.; Stewart, J. R.; Cowlam, N.; Al-Heniti, S.; Kiss, L. F.; Kemény, T., *J. Phys. Condens. Matter* **2003**, *15*, 675–691
16. Hafner, J.; Tegze, M.; Becker, Ch., *Phys. Rev. B* **1994**, *49*, 285–298
17. Hausleitner, Ch.; Hafner, J., *Phys. Rev. B* **1993**, *47*, 5689–5709
18. Gupta, A.; Bhandari, D.; Saxena, N. S., *Ind. J. Pure & Appl. Phys*. **1998**, *36*, 366
19. Saxena, N. S.; Non-Cryst, J., *Sol*. **1996**, *196*, 37
20. Harrison W. A., Elementary Electronic Structure, World Scientific, Singapore (1999)
21. Taylor, R.; Phys, J., *F: Met. Phys*. **1978**, *8*, 1699–1702
22. Ichimaru, S.; Utsumi, K., *Phys. Rev. B* **1981**, *24*, 7385–7388
23. Farid, B.; Heine, V.; Engel, G.; Robertson, I. J., *Phys. Rev. B* **1993**, *48*, 11602–11621
24. Sarkar, A.; Sen, D. S.; Haldar, S.; Roy, D., *Mod. Phys. Lett. B* **1998**, *12*, 639
25. Sarkar, A.; Haldar, S.; Roy, D.; Sen, D., *Acta Physiol. Pol*. **2004**, *A106*, 497
26. Takeno, S.; Goda, M., *Prog. Theor. Phys*. **1971**, *45*, 331–352
27. Takeno, S.; Goda, M., *Prog. Theor. Phys*. **1972**, *47*, 790–806
28. Shukla, M. M.; Campanha, J. R., *Acta Physiol. Pol*. **1998**, *A94*, 655
29. Wills, J. M.; Harrison, W. A., *Phys. Rev. B* **1983**, *28*, 4363–4373
30. Hafner, J.; Heine, V.; Phys, J., *F: Met. Phys*. **1983**, *13*, 2479–2501
31. Kovalenko, N. P.; Krasny, Y. P., *Physica B* **1990**, *162*, 115–121
32. Hausleitner, Ch.; Turek, I.; Non-Cryst, J., *Sol*. **1993**, *156–158*, 210
33. Bretonnet, J. L.; Derouiche, A., *Phys. Rev. B* **1990**, *43*, 8924–8929
34. Thorpe, M. F.; Non-Cryst, J., *Sol*. **1983**, *57*, 355